Research Article | Vol. 14, No. 2 / 1 Feb 2024 / Optical Materials Express 435
Optical Materials EXPRESS

Thermo-optic characterization of SU-8 at cryogenic temperature

Trisha Chakraborty,[1,2,*] Oscar A. Jimenez Gordillo,[3] Michael Barrow,[1,2] Alan R. Kramer,[2] Michal Lipson,[4] Thomas E. Murphy,[1] and Karen E. Grutter[1,2]

[1]Department of Electrical and Computer Engineering, University of Maryland, College Park, MD 20742, USA
[2]Laboratory for Physical Sciences, College Park, MD 20740, USA
[3]Department of Electronics, Information and Bioengineering, Politecnico di Milano, 20133 Milano, Italy
[4]Department of Electrical Engineering, Columbia University, New York, NY 10027, USA
[*]tchakrab@umd.edu

Abstract: We measured the optical transmission through an SU-8 microring resonator inside a cryostat and analyzed the shift of the resonant wavelengths to determine the thermo-optic behavior around a wavelength of 1600 nm. As the temperature was decreased from room temperature (RT) to 3K, the refractive index of crosslinked SU-8 was measured to increase from 1.571 to 1.584, while the thermo-optic coefficient decreased by two orders of magnitude.

1. Introduction

Polymer-based resists are a potentially convenient alternative to traditional dielectric waveguide materials. As they are patterned solely using existing lithography processes, no etch processes or substantial thermal processing are required to incorporate them into a film stack. SU-8, a negative-tone electron-beam and photolithography resist, is particularly attractive as a photonic material [1]. This bisphenol A novolac epoxy-based resist, originally developed for patterning microelectronics can be used to create films over a very wide thickness range (0.5 μm - 500 μm), enabling pattering of high aspect-ratio (>190:1) structures with smooth sidewalls [2,3]. It has a wide transparency window for wavelengths greater than 400 nm [4] and less than 1.6 dB/cm propagation loss around 1550 nm [5] has been demonstrated in SU-8 waveguides. As a result, SU-8 has been utilized in a wide range of photonic devices, including filters [6,7], sensors [8,9], modulators [10], and quantum dot-based single-photon sources [11]. Furthermore, SU-8 can be cross-linked using 2-photon polymerization to realize 3D nano-structures, such as topological photonic devices [12], MEMS transducers [13], microlenses [14], and photonic wire bonds [15].

These demonstrations of SU-8, especially in 3D photonic wirebonds and quantum dot-based single-photon sources, point toward further promising use cases as an optical material in quantum computing and superconducting applications. However, in order to be effectively used in these applications, SU-8's optical properties at cryogenic temperatures must be well-understood, and no cryogenic optical characterizations of SU-8 have been reported to date. In this work, we measure the variation of the refractive index and thermo-optic coefficient of SU-8 with respect to temperature from room temperature to 3 K using an on-chip SU-8 microring resonator operating in the C and L bands (1520 nm to 1625 nm).

2. Device design

The device we used to characterize the thermo-optic coefficient of SU-8 is a microring evanescently coupled to a bus waveguide, both made of SU-8 on 3 μm of SiO_2 (Fig. 1(a)). The cross-sectional

#509626 https://doi.org/10.1364/OME.509626
Journal © 2024 Received 16 Oct 2023; revised 21 Dec 2023; accepted 21 Dec 2023; published 24 Jan 2024

Optical Materials EXPRESS

dimensions of the waveguide were designed to be 2.5 μm in width and 2 μm in thickness supporting single-mode TE propagation around an optical wavelength of 1550 nm (Fig. 1(b)).

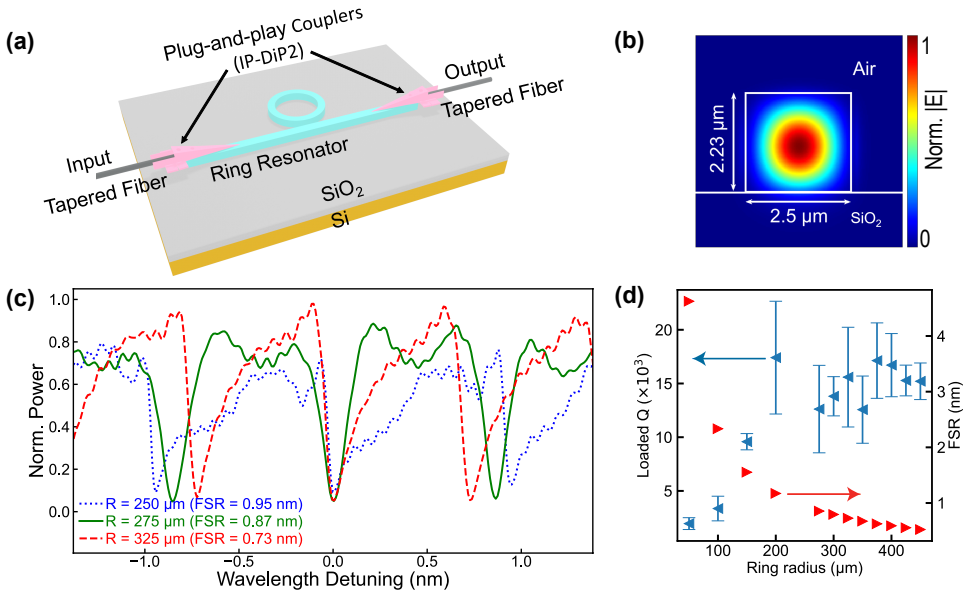

Fig. 1. (a) Diagram of the SU-8 microring resonator with input and output plug-and-play couplers (b) Simulated TE mode profile of the SU-8 waveguide. (c) Transmission spectrum of SU-8 ring resonator devices with three different ring radii. (d) Measured loaded Q and free spectral range (FSR) with respect to ring radius. Loaded optical quality factor Q comes from Lorentzian fits of the resonances, and error bars indicate the standard deviation of Q for all the measured resonances across the C and L bands.

To select the optimal radius of the microring, we fabricated and characterized devices with various ring radii. Figure 1(c) shows the transmission spectra of three edge-coupled devices with 250 μm, 275 μm and 325 μm ring radius. As expected, optical quality factor Q decreased as the microring radius decreased due to excess bending loss (Fig. 1(d)). However, a larger microring radius results in a smaller free spectral range (FSR) causing possible ambiguity in the detection of resonant wavelength shift. In order to ensure a larger FSR while maintaining high Q, we chose a microring radius of 275 μm. We chose the coupling gap of 600 nm between the microring and the bus waveguide, so that the ring resonator operates in the undercoupled regime. In this regime, the presence of the adjacent bus waveguide makes a negligible contribution to the resonance condition, so that any observed spectral shift in the resonant wavelength can be entirely attributed to a shift in the refractive index of the SU-8 microring and its SiO_2 under-cladding.

On-chip coupler structures printed via 3D direct laser writing is one of the newly emerging coupling schemes with high potential [16]. In order to enable fiber-to-chip coupling to the device without active alignment throughout the temperature range, we designed 3D input and output funnel and tapered waveguide structures made of the 2-photon polymerizable resin IP-Dip2 to couple light into and out of the the bus waveguide. Our design is adapted from ref. [17], with significant modification of the coupler structure to enable adiabatic evanescent coupling to the SU-8 bus waveguide instead of using grating couplers. These plug-and-play couplers provide mechanical stability to the input and output optical fibers and maintain efficient optical coupling without relying on active mechanical alignment throughout the cryogenic thermal cycle. Figure 1(a) is a 3D schematic of the ring resonator structure with both input and output couplers. A brief description of the coupler design is discussed in ref. [18].

Optical Materials EXPRESS

3. Fabrication and packaging

To fabricate the ring resonator device, we spun 2 μm thick SU-8 2002 on 3 μm of thermal SiO_2 on a Si substrate. A 100 kV electron-beam lithography system with an exposure dosage of 10 μJ/cm^2 was used to pattern the SU-8 resist layer. Our ellipsometry (see Sec. 4 for more details), atomic force microscopy, and surface profilometer measurements indicated a final device height of 2.23 μm. Figure 2(a) is an optical microscope image of the ring resonator structure with a 3D coupler at one end of the bus waveguide. To define this 3D plug-and-play coupler on the SU-8 waveguide, we used 2-photon lithography to polymerize the negative-tone resin IP-Dip2. The inset shows a colorized SEM image of the coupler with tapered fiber entering the supporting funnel and the 3D taper printed on top of the SU-8 waveguide. After development, a blanket UV light exposure was used to ensure complete cross-linking of the plug-and-play coupler structures.

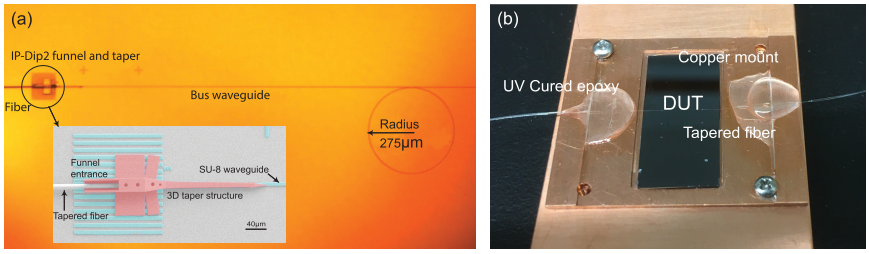

Fig. 2. (a) Microscope image of ring resonator device with fiber inserted in one of the plug-and-play coupler funnels. (inset) Colorized SEM image of the plug-and-play coupler funnel and 3D taper structure on top of SU-8 waveguide. (b) Image of packaged device with input and output tapered fibers affixed on a copper mount.

In order to characterize the microring resonators, tapered single-mode fibers with an approximate tip diameter of 10 μm were inserted in the entrance ports of the 3D funnels. These funnels mechanically guide the fiber tip into alignment with the tapered IP-Dip2 waveguides at the ends of the SU-8 bus waveguide to adiabatically couple light in and out. Using thermally-conductive silver-impregnated room-temperature-vulcanizing (RTV) paste, we attached the sample to a copper mount to ensure thermal contact inside cryostat. After insertion, both input and output fibers were affixed to the copper mount using UV-curable epoxy as shown in Fig. 2(b). No further alignment was required once the device was mounted inside the cryostat.

4. Material characterization at room temperature

The cryogenic characterization method depends upon knowledge of the room temperature refractive index, which serves as a starting point when the sample is cooled to low temperature. For this purpose, we used variable angle spectroscopic ellipsometry (VASE) to precisely measure the refractive index of cross-linked SU-8 films, $n_{\text{SU-8}}$ at room temperature. VASE is an optical technique that determines changes in the polarization state of reflected light at discrete wavelengths due to the influence of sample material properties. Two parameters are required to describe the general state of polarization [19], the relative phase Δ and ratio of orthogonal electric field components Ψ at each measured wavelength λ. These are related to the Fresnel reflection coefficients [20] of a simple single film on substrate sample by:

$$\tan(\Psi)e^{i\Delta} = \frac{R_p}{R_s}. \tag{1}$$

A complete treatment of the theory can be found in Azzam and Bashara [21].

Although there are examples in the literature of room-temperature VASE characterization of SU-8 [22,23], we needed a precise value of $n_{\text{SU-8}}$ of our own material with thickness around

Optical Materials EXPRESS

2 μm. Unlike previous VASE measurements, ours included reflections from the substrate, enabling characterization of the effective optical properties of the full thickness of SU-8 instead of just at the air / SU-8 interface. Our measured $n_{\text{SU-8}}$ around 1550 nm is comparable to the previously-reported values [23].

Samples are prepared specifically for ellipsometric characterization by spin-coating SU-8 2002 on a plain Si wafer using the same procedure as for our microring devices. We then cross-linked the SU-8 using a blanket UV-light exposure. Cross-linked SU-8 films or patterned structures have shown long term chemical stability and cross sample repeatability [24] and therefore this method of room temperature characterization of optical constants from the ellipsometry prepared sample is a robust method of determining the optical constants of the microring devices.

VASE measurements are performed at discrete points from 190 nm to 1700 nm. A simple model representing a thin film atop of a semi-infinite substrate is used. The $[\Delta_\lambda, \Psi_\lambda]$ data set collected is the solution to an equation parameterized by the complex $n_{\text{SU-8}}(\lambda)$ of the SU-8 and film thickness, d. Optical constants for the silicon substrate are fixed at values as determined by Herzinger *et al.* [25]. Inclusion of surface roughness and interface non-uniformity (substrate surface roughness, native oxide layer, material mixing, interface induced strain, etc.) are neglected in this model as the errors associated with those parameters exceed the values themselves. The thickness of this particular SU-8 film was 2.2 μm and therefore inclusion of these other model features represent a very small component in an effective medium approximation. $n_{\text{SU-8}}(\lambda)$ of the SU-8 are characterized by the Kramers-Kronig consistent Cody-Lorentz [26] dispersion relation. The Cody-Lorentz model is also paired with three Gaussian oscillators to describe the three absorption peaks present in the UV (4.0 eV - 6.0 eV) region of the spectrum.

The model agreement with the measured data can be seen in Fig. 3. Since the thick film does incorporate a reflected signal from the substrate/film interface, the model needs to compensate for depolarization effects. Similarly, bandwidth (wavelength smearing) and thickness non-uniformity (across the beam) are also parameterized and found to be 2.5 nm and 1% respectively. While there is some disagreement between model and measured Δ and Ψ in the UV region, it is too small to be easily seen in Fig. 3, and is likely attributed to the stronger absorption occurring in the UV — a feature that also makes SU-8 less suitable for photonic applications in this regime. The three Gaussian oscillators serve to anchor the entire spectrum increasing the reliability of the fit in the NIR region.

Figure 4 shows the derived optical constants for the cross-linked SU-8 film using the Cody-Lorentz dispersion relation. This model parameterizes the optical band gap, such that, for wavelengths longer than 371.4 nm, k is set to zero. From this model the refractive index at 1600 nm is $n_{\text{SU-8}} = 1.571020 \pm 0.000003$, where the uncertainty is derived from the fit.

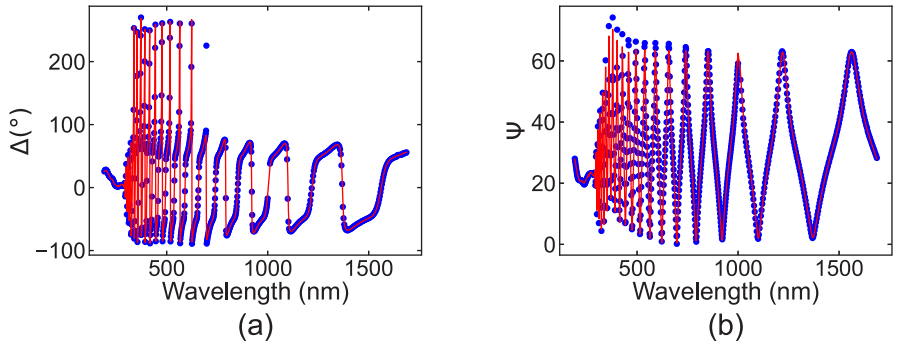

Fig. 3. Measured and model Δ (a) and Ψ (b) in blue dots and red line respectively for the 2.2 μm thick SU-8 film.

Optical Materials EXPRESS

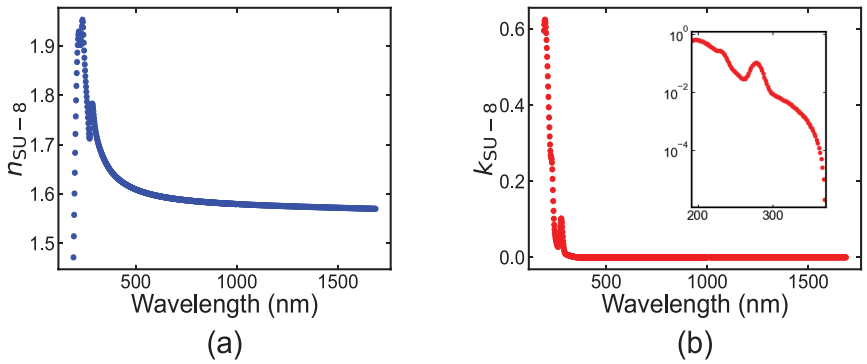

Fig. 4. (a) Derived index of refraction, $n_{SU\text{-}8}$ and (b) Extinction coefficient, $k_{SU\text{-}8}$ for the 2.2 μm thick SU-8 film. (inset) $k_{SU\text{-}8}$ in log scale for a wavelength range of 191.4-371.4 nm.

5. Device characterization

Figure 5(a) shows the packaged device mounted on the 3 K stage of the cryostat. After mounting the device, the 3 K stage was enclosed in three layers of shielding to maintain stable temperature. The cryogenic chamber was cooled using a closed-cycle Gifford-McMahon refrigerator. A tunable laser source and a swept wavelength spectrometer were connected to the the device via fiber-optic feedthroughs (Fig. 5(b)). We used a three-paddle polarization controller to ensure TE polarization at the input of the bus waveguide.

We recorded the transmission spectra through the device as it cooled down to 3 K from room temperature over a period of approximately 10 h (Fig. 5(c)). The temperature was measured using a calibrated thin film resistance temperature sensor mounted on the cold plate.

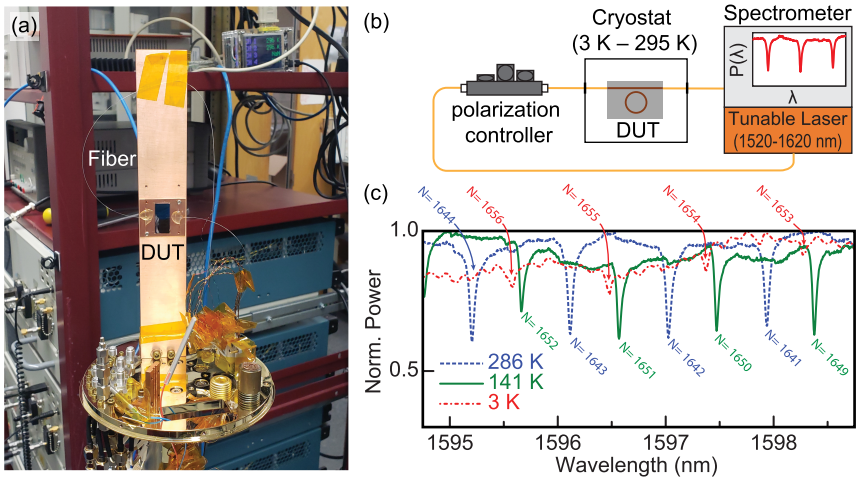

Fig. 5. (a) Image of device mounted inside cryostat on a copper mount. (b) Schematic of the characterization setup (DUT = device under test). (c) Normalized transmission spectrum of the ring resonator at 286 K, 141 K, and 3 K.

Optical Materials EXPRESS

6. SU-8 results and analysis

The SU-8 microring's resonant wavelength shifted red as it cooled, slowing significantly below 30 K (Fig. 6(a)). Based on these measurements, we calculated the mode effective index n_{eff} for each resonance of order N as it cooled using the following equation [27]:

$$\lambda_N = \frac{2\pi R n_{\text{eff}}(\lambda_N, T)}{N}, \tag{2}$$

where λ_N is the resonant wavelength of order N and R is the ring radius. In order to determine N for a particular resonance, we first solved for the room-temperature n_{eff} of the fundamental TE mode of the SU-8 waveguide cross-section using Marcatili's method for a rectangular dielectric waveguide [28,29], where we have used the wavelength-dependent $n_{\text{SU-8}}$ obtained from the ellipsometry measurement (Sec. 4) and room-temperature, wavelength-dependent n_{SiO_2} from Ref. [30]. As an example, for the mode that was around 1592 nm at room temperature, the calculated room-temperature $n_{\text{eff}} = 1.5173 \pm 0.0007$. Substituting this value into Eq. (2), we found $N = 1647 \pm 1$. We then used this resonance order in Eq. (2) to calculate n_{eff} from the measured resonant wavelengths at all temperatures.

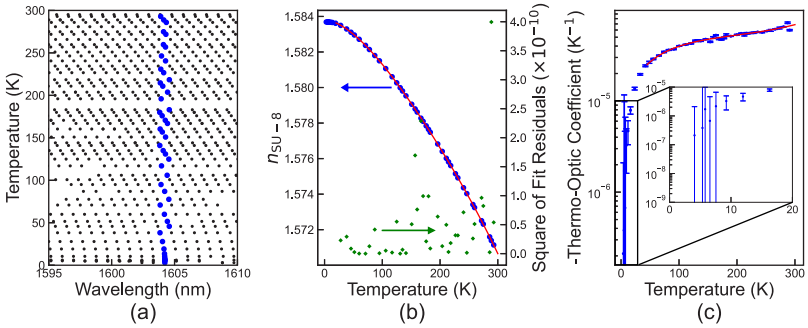

Fig. 6. (a) Resonant wavelength vs. temperature for multiple orders of resonance. Analysed resonant wavelengths within 1604.2 ± 0.4 nm range are marked in blue dots. See Data File 1 for underlying values. (b) Refractive index of SU-8 with respect to temperature extracted from the measured resonant wavelength range. A fourth-order fit above 20 K is shown as red line with the square of the fit residuals as green diamonds. (c) Blue dots indicate the negative thermo-optic coefficient values for the whole temperature range obtained from point-to-point linear interpolation of the measured $n_{\text{SU-8}}(T)$. Uncertainty is from the wavelength accuracy of the swept wavelength spectrometer. Negative of the TOC of SU-8 above 20 K, derived from the fit of the measured $n_{\text{SU-8}}(T)$ is shown as a red line.

To isolate thermo-optic changes in refractive index from the effects of chromatic dispersion, we selected points with a specific wavelength range, 1604 ± 0.4 nm, as shown in Fig. 6(a). We then extracted $n_{\text{SU-8}}$ at each selected point. As found from eigenmode simulation, less than 5% of the waveguide mode power overlaps with the SiO_2 substrate. We accounted for this contribution in our analysis by using the temperature-dependent n_{SiO_2} reported in literature [30]. We again used Marcatili's method to solve for $n_{\text{SU-8}}$ at different temperatures for the corresponding n_{eff} values (Fig. 6(b)). We note that an eigenmode simulation software could also be used to iteratively find $n_{\text{SU-8}}$ from n_{eff}.

The thermo-optic coefficient of the mode $\frac{\partial n_{\text{eff}}}{\partial T}$ could also be calculated directly from the change in resonant wavelength with temperature: $\frac{\partial n_{\text{eff}}}{\partial T} = \frac{n_g}{\lambda}\frac{\mathrm{d}\lambda}{\mathrm{d}T}$, where n_g is the group index, which could be approximated from the free spectral range of the resonator. A similar relationship would give the thermo-optic coefficient of the core material, but this requires a measurement or estimate of the material group index, which need not match the waveguide group index. Moreover, this

Optical Materials EXPRESS

approach does not directly give the refractive index $n_{\text{eff}}(T)$ and $n_{\text{SU-8}}(T)$, which relies on an estimate of the mode order N.

In order to describe the general trend of the data, we then fit $n_{\text{SU-8}}(T)$ to the following fourth-order polynomial:

$$n(T) = p_1 T^4 + p_2 T^3 + p_3 T^2 + p_4 T + p_5 \tag{3}$$

This fit describes the data fairly well for temperatures above 20 K with fitting parameters: $p_1 = (-1.01 \pm 0.09) \times 10^{-12}$ K^{-4}, $p_2 = (7.6 \pm 0.6) \times 10^{-10}$ K^{-3}, $p_3 = (-2.7 \pm 0.1) \times 10^{-7}$ K^{-2}, $p_4 = (-5.3 \pm 1.2) \times 10^{-6}$ K^{-1}, and $p_5 = 1.58384 \pm 0.00003$. This polynomial fit above 20 K is shown as a red line in Fig. 6(b) along with the square of the fit residuals. We differentiated this polynomial with respect to temperature to extrapolate the thermo-optic coefficient (TOC) $\frac{\partial n_{\text{SU-8}}}{\partial T}$ of SU-8 above 20 K (Fig. 6(c)). At room temperature, this fit gives $\frac{\partial n_{\text{SU-8}}}{\partial T} = (-6.746 \pm 0.055) \times 10^{-5}$ K^{-1}.

As temperature approaches 0 K and the vibrational transitions freeze out, we expect the index of refraction to level off and the TOC to approach zero [31]. This rapid decrease of TOC at base temperature can be explained from a thermodynamic point of view as reported in the literature [32,33]. The leveling-off of $n_{\text{SU-8}}$ is not captured by the fourth-order polynomial fit, but it is evident that the TOC is decreasing rapidly below 20 K. We find that $n_{\text{SU-8}}$ converges to about 1.584 at the lowest temperatures in our measurement. In order to extract the TOC for the whole temperature range we did a point-to-point linear interpolation of the measured $n_{\text{SU-8}}(T)$ data (as shown in Fig. 6(c) with blue dots) and found that the TOC at 4 K is on the order of -1×10^{-7} K^{-1}.

To compare to previous work, the only experimentally-measured room-temperature TOC of SU-8 reported in the literature is -1.1×10^{-4} K^{-1} [34], which is comparable to our room-temperature measurement in terms of order of magnitude. The discrepancy can likely be attributed to differences in the processing of the SU-8 (their film had $n_{\text{SU-8}} = 1.565$ at room temperature, ≈ 0.006 lower than ours) and to the fact that their measurement was taken over an elevated temperature range (293 K to 333 K).

7. Validation with silicon

To validate our experimental process and data analysis method for extracting the temperature-dependent refractive index of SU-8, we also characterized a silicon-on-insulator (SOI) microring resonator device with similar plug-and-play couplers. This Si resonator had a 30 μm ring radius with a waveguide width of 0.95 μm and thickness of 0.22 μm. It was clad on the bottom and sides with SiO_2 and on the top with air. We packaged the device with tapered fibers at the input and output ports in the same fashion and characterized the temperature-induced shifting of the microring's resonances, shown in Fig. 7(a). We analyzed the wavelength shift and extracted the refractive index of Si (n_{Si}) using the same procedure as for SU-8 (Sec. 6). Our extracted values for n_{Si} are in excellent agreement to the temperature-dependent refractive index reported by Frey *et al.* [35].

We fit our $n_{\text{Si}}(T)$ data to polynomials to describe the temperature dependence of the index of refraction (Fig. 7(c)) of Si. For most of the temperature range (above 45 K), we found that a third-order polynomial (Eq. (4)) described the data best:

$$n(T) = p_1 T^3 + p_2 T^2 + p_3 T + p_4, \tag{4}$$

where coefficients $p_1 = (-4.15 \pm 1.95) \times 10^{-10}$ K^{-3}, $p_2 = (5.25 \pm 1.02) \times 10^{-7}$ K^{-2}, $p_3 = (-1.69 \pm 1.61) \times 10^{-5}$ K^{-1} and $p_4 = 3.4464 \pm 0.0007$. From this fit, we determined the TOC of Si at room temperature to be $(1.84 \pm 0.07) \times 10^{-4}$ K^{-1} which is consistent with that reported in the literature (1.8×10^{-4} K^{-1}) [35,36]. To extract empirical values across the full temperature

Optical Materials EXPRESS

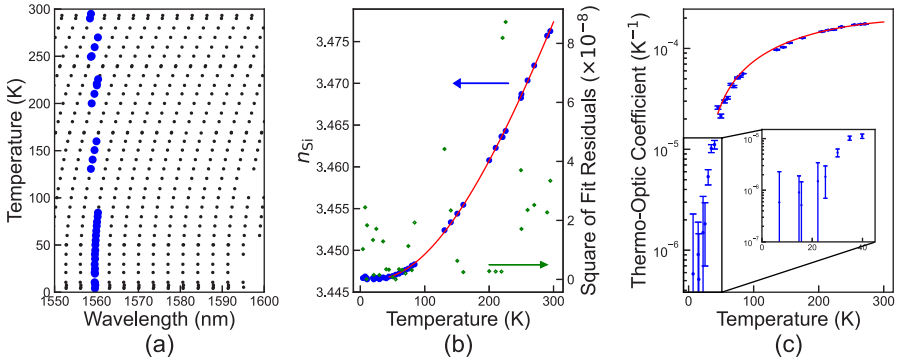

Fig. 7. (a) Resonant wavelength vs. temperature for multiple orders of resonance in a Si microring resonator. Analyzed resonant wavelength within 1559.4 ± 1.0 nm range is marked in blue See Data File 2 for underlying values. (b) Refractive index of Si with respect to temperature extracted from the measured resonant wavelength range. A third-order fit above 45 K is shown as a red line with the square of the fit residuals as green diamonds. (c) Blue dots indicate the thermo-optic coefficient values for the whole temperature range obtained from point-to-point linear interpolation of the measured $n_{Si}(T)$. Uncertainty is from the wavelength accuracy of the swept wavelength spectrometer. The TOC of Si above 45 K, derived from the fit of the measured $n_{Si}(T)$, is shown as a red line.

range, we performed the same point-to-point linear interpolation of the measured $n_{Si}(T)$. At around 6 K, we measured the TOC of Si to be on the order of 10^{-7} K^{-1}, which is comparable to that reported in the literature [36]. Such consistency in our measured data to previously reported refractive index and TOC values of Si across this temperature range confirms the validity of our approach for characterizing the thermo-optic behavior of SU-8 under cryogenic conditions.

8. Conclusion

In this work, we fabricated and packaged an SU-8 microring resonator device, and characterized it inside a cryostat to determine the shift of the optical resonant wavelengths with respect to temperature. From this, we extracted the refractive index and thermo-optic coefficient of SU-8 down to 4 K. As with other polymers [37], our experimental results show that SU-8 has a negative thermo-optic coefficient throughout the temperature range 3 K to 300 K. At room temperature the measured value of the refractive index and TOC of cross-linked SU-8 are 1.571 and $(-6.746 \pm 0.055) \times 10^{-5}$ K^{-1} respectively. The absolute value of this $\frac{\partial n_{SU\text{-}8}}{\partial T}$ decreased by over two orders of magnitude with 0.8 % increase in refractive index of SU-8 as the device cooled down to the base temperature (3 K). We also applied the same analysis technique to the temperature-dependent resonant wavelength shift of a silicon microring resonator to extract the optical properties of silicon from room to cryogenic temperature. Agreement of our measured values of the refractive index and TOC of Si to values reported in the literature validate this measurement technique.

In addition to its many demonstrated room-temperature photonic applications, SU-8 is a promising material for passive integrated photonic components in quantum and superconducting computing. Our measurement of the thermo-optic behavior of this material over a temperature range of base to room temperature will be critical for designing future SU-8 devices for cryogenic operation.

Disclosures. The authors declare no conflicts of interest.

Data availability. Data presented in Fig. 6(a) and Fig. 7(a) are available in Data File 1 and Data File 2.

Optical Materials EXPRESS

References

1. W. D. Hinsberg and G. M. Wallraff, "Lithographic resists," in *Kirk-Othmer Encyclopedia of Chemical Technology*, (John Wiley & Sons, Ltd, 2005).
2. A. del Campo and C. Greiner, "SU-8: A photoresist for high-aspect-ratio and 3D submicron lithography," J. Micromech. Microeng. **17**(6), R81–R95 (2007).
3. R. Yang and W. Wang, "A numerical and experimental study on gap compensation and wavelength selection in UV-lithography of ultra-high aspect ratio SU-8 microstructures," Sens. Actuators, B **110**(2), 279–288 (2005).
4. K. K. Tung, W. H. Wong, and E. Y. B. Pun, "Polymeric optical waveguides using direct ultraviolet photolithography process," Appl. Phys. A **80**(3), 621–626 (2005).
5. X. Wang, J. Meng, Y. Yue, *et al.*, "Fabrication of single-mode ridge SU-8 waveguides based on inductively coupled plasma etching," Appl. Phys. A **113**(1), 195–200 (2013).
6. C. A. Leal-Sevillano, J. R. Montejo-Garai, M. Ke, *et al.*, "A Pseudo-Elliptical Response Filter at W-Band Fabricated With Thick SU-8 Photo-Resist Technology," IEEE Microw. Wireless Compon. Lett. **22**(3), 105–107 (2012).
7. K. Jiang, M. J. Lancaster, I. Llamas-Garro, *et al.*, "SU-8 Ka-band filter and its microfabrication," J. Micromech. Microeng. **15**(8), 1522–1526 (2005).
8. Y. Xin, G. Pandraud, Y. Zhang, *et al.*, "Single-Mode Tapered Vertical SU-8 Waveguide Fabricated by E-beam Lithography for Analyte Sensing," Sensors **19**(15), 3383 (2019).
9. N. Pelletier, B. Bêche, N. Tahani, *et al.*, "SU-8 waveguiding interferometric micro-sensor for gage pressure measurement," Sens. Actuators, A **135**(1), 179–184 (2007).
10. E. Nitiss, A. Tokmakovs, K. Pudzs, *et al.*, "All-organic electro-optic waveguide modulator comprising SU-8 and nonlinear optical polymer," Opt. Express **25**(25), 31036–31044 (2017).
11. L. P. Nuttall, F. S. F. Brossard, S. A. Lennon, *et al.*, "Optical fabrication and characterisation of SU-8 disk photonic waveguide heterostructure cavities," Opt. Express **25**(20), 24615–24622 (2017).
12. J. Schulz, S. Vaidya, and C. Jörg, "Topological photonics in 3D micro-printed systems," APL Photonics **6**(8), 080901 (2021).
13. O. Tricinci, M. Carlotti, A. Desii, *et al.*, "Two-step MEMS microfabrication via 3D direct laser lithography," Proc. SPIE **11696**, 116960J (2021).
14. H. E. Williams, D. J. Freppon, S. M. Kuebler, *et al.*, "Fabrication of three-dimensional micro-photonic structures on the tip of optical fibers using SU-8," Opt. Express **19**(23), 22910–22922 (2011).
15. N. Lindenmann, G. Balthasar, D. Hillerkuss, *et al.*, "Photonic wire bonding: a novel concept for chip-scale interconnects," Opt. Express **20**(16), 17667–17677 (2012).
16. H. Gehring, M. Blaicher, W. Hartmann, *et al.*, "Low-loss fiber-to-chip couplers with ultrawide optical bandwidth," APL Photonics **4**(1), 010801 (2019).
17. O. A. J. Gordillo, S. Chaitanya, Y.-C. Chang, *et al.*, "Plug-and-play fiber to waveguide connector," Opt. Express **27**(15), 20305–20310 (2019).
18. T. Chakraborty, O. A. J. Gordillo, M. Barrow, *et al.*, "Thermo-Optic Characterization of SU-8 at Cryogenic Temperature," in *Conference on Lasers and Electro-Optics*, (Optica Publishing Group, 2022), p. SF3O.7.
19. R. D. Guenther, *Modern Optics* (Oxford University Press, 2015), 2nd ed. Chap. 2.
20. M. Born and E. Wolf, *Principles of Optics: Electromagnetic Theory of Propagation, Interference and Diffraction of Light* (Cambridge University Press, 1999), 7th ed. Sec. 15.
21. R. M. A. Azzam and N. M. Bashara, *Ellipsometry and Polarized Light* (North Holland, 1977).
22. W. R. Folks, J. Ginn, D. Shelton, *et al.*, "Spectroscopic ellipsometry of materials for infrared micro-device fabrication," Sens. Actuators, A **5**(5), 1113–1116 (2008).
23. G. H. Major, S. C. Chapman, J. T. Chapman, *et al.*, "Spectroscopic ellipsometry of SU-8 photoresist from 190 to 1680 nm (0.740–6.50 eV)," Surf. Interface Anal. **53**(1), 5–13 (2021).
24. J. Hammacher, A. Fuelle, J. Flaemig, *et al.*, "Stress engineering and mechanical properties of SU-8-layers for mechanical applications," Microsyst. Technol. **14**(9-11), 1515–1523 (2008).
25. C. M. Herzinger, B. Johs, W. A. McGahan, *et al.*, "Ellipsometric determination of optical constants for silicon and thermally grown silicon dioxide via a multi-sample, multi-wavelength, multi-angle investigation," J. Appl. Phys. **83**(6), 3323–3336 (1998).
26. A. S. Ferlauto, G. M. Ferreira, J. M. Pearce, *et al.*, "Analytical model for the optical functions of amorphous semiconductors from the near-infrared to ultraviolet: Applications in thin film photovoltaics," J. Appl. Phys. **92**(5), 2424–2436 (2002).
27. V. Donzella, A. Sherwali, J. Flueckiger, *et al.*, "Design and fabrication of SOI micro-ring resonators based on sub-wavelength grating waveguides," Opt. Express **23**(4), 4791–4803 (2015).
28. E. A. J. Marcatili, "Dielectric rectangular waveguide and directional coupler for integrated optics," Bell Syst. Tech. J. **48**(7), 2071–2102 (1969).
29. S. L. Chuang, *Physics of Optoelectronic Devices*, Wiley Series in Pure and Applied Optics (John Wiley, 1995), 1st ed. Chap. 7.
30. D. B. Leviton and B. J. Frey, "Temperature-dependent absolute refractive index measurements of synthetic fused silica," Proc. SPIE **6273**, 62732K (2006).
31. M. E. Thomas, "Temperature dependence of the complex index of refraction," in *Handbook of Optical Constants of Solids*, E. D. Palik, ed. (Academic Press, 1998), pp. 177–201.

Optical Materials EXPRESS

32. N. G. C. Astrath, J. H. Rohling, A. N. Medina, *et al.*, "Time-resolved thermal lens measurements of the thermo-optical properties of glasses at low temperature down to 20K," Phys. Rev. B **71**(21), 214202 (2005).
33. N. G. C. Astrath, A. N. Medina, A. C. Bento, *et al.*, "Time resolved thermal lens measurements of the thermo-optical properties of Nd_2O_3-doped low silica calcium aluminosilicate glasses down to 4.3K," J. Non-Cryst. Solids **354**(2-9), 574–579 (2008).
34. P. Rabiei, W. Steier, C. Zhang, *et al.*, "Polymer micro-ring filters and modulators," J. Lightwave Technol. **20**(11), 1968–1975 (2002).
35. B. J. Frey, D. B. Leviton, and T. J. Madison, "Temperature-dependent refractive index of silicon and germanium," Proc. SPIE **6273**, 62732J (2006).
36. J. Komma, C. Schwarz, G. Hofmann, *et al.*, "Thermo-optic coefficient of silicon at 1550 nm and cryogenic temperatures," Appl. Phys. Lett. **101**(4), 041905 (2012).
37. Z. Zhang, P. Zhao, P. Lin, *et al.*, "Thermo-optic coefficients of polymers for optical waveguide applications," Polymer **47**(14), 4893–4896 (2006).